analytical chemistry

pubs.acs.org/ac Article

A Novel Ratiometric Electrochemical Biosensor Using Only One Signal Tag for Highly Reliable and Ultrasensitive Detection of miRNA-21

Lingqi Kong, Hao Li, Xiaolong Zhang, Ying Zhuo, Yaqin Chai,* and Ruo Yuan*

Cite This: *Anal. Chem.* 2022, 94, 5167−5172 Read Online

ACCESS | Metrics & More | Article Recommendations | Supporting Information

ABSTRACT: Herein, a novel ratiometric electrochemical biosensor with methylene blue (MB) as the only one signal tag was proposed for highly reliable and ultrasensitive detection of microRNA-21 (miRNA-21) under the assistance of an intelligent target-induced dual signal amplification (T-DSA). First, a small amount of target miRNA-21 could produce abundant mimic targets DNA S1 and Zn^{2+} through target-induced recycle and acid dissolution, respectively. Then, S1 triggered rolling circle amplification (RCA) to generate functional DNA nanospheres (DSP) encoded by DNAzyme and substrate sequence for loading numerous signal tag MB with a remarkable electrochemical signal (signal on), and the Zn^{2+} cofactor mediated the nonviolent DNAzyme-catalyzed cleavage of DSP to sharply release MB with obviously reduced electrochemical responses (signal off). Impressively, our strategy could controllably load and release the only signal tag MB through the well-designed DSP to effectively avoid the false positive responses caused by the non-ideal upright state of DNA probes connected to electrodes in traditional distance-dependent signal adjustment ratiometric strategies with two different signal tags. Meanwhile, with the aid of innovative T-DSA recycle and RCA-produced functional DSP, the detection sensitivity of this sensing platform was significantly improved. As a result, the proposed biosensor successfully realized highly reliable and ultrasensitive detection of miRNA-21 with a detection limit down to 26.7 aM, which shows exceptional promise in biological analysis and medical diagnosis.

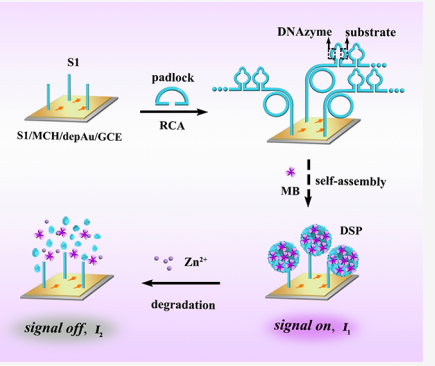

INTRODUCTION

MicroRNAs (miRNAs), as representative nucleic acid biomarkers, are a group of endogenous, noncoding, single-stranded RNAs that perform an incomparable role in regulating genetic expression and cellular processes involving proliferation, differentiation, and apoptosis.[1−4] To date, many research studies have proven that various major diseases are associated with the abnormal expression of miRNA.[5−9] Therefore, considerable efforts have been devoted to establish sensitive and specific miRNA sensing strategies to develop the early diagnosis of cancers and targeted anticancer drugs.[10−14] Nevertheless, owing to the low abundance, small size, and high sequence homology of miRNA fragments, most biosensors suffered from different troubles in practical applications, involving poor robustness, reproducibility, accuracy, and reliability.[15−17]

Recently, researchers have exploited many new sensing technologies to overcome the above shortcomings, in which the electrochemical ratiometric biosensor has attracted considerable interest due to its ability to effectively deduct systematic or intrinsic disturbances derived from micro-environments.[18−20] Usually, the target-induced distance change between two different signal tags to an electrode surface is the most universal strategy to construct ratiometric biosensors.[21,22] Although this strategy had the inherent advantages of the conventional ratiometric method, the local disorder of the DNA on the electrode surface, involving DNA slant, entanglement, rotational movement, elastic bending, and nonspecific bindings, might disturb the expected change in the distance between the signal tags and electrode surface, thereby further interfering the performance of distance-dependent ratiometric biosensors.[23−25] Moreover, in these strategies, the detection sensitivity was greatly limited due to the lack of target-related signal amplification. Therefore, exploring a novel electrochemical ratiometric method to overcome the existing shortcomings is an urgent necessity.

In this study, an innovative ratiometric electrochemical sensing platform with only one redox label was exploited for accurate and ultrasensitive detection of target miRNA-21 with the help of an ingenious target-induced dual signal amplification (T-DSA) recycle and functional DNA nano-

Received: January 13, 2022
Accepted: March 7, 2022
Published: March 17, 2022

https://doi.org/10.1021/acs.analchem.2c00190
Anal. Chem. 2022, 94, 5167−5172

Scheme 1. Principle of the Reliable and Ultrasensitive Ratiometric Electrochemical Biosensor: (A) Target-Initiated Dual Signal Amplification and (B) Electrode Interface Modifications and Signal Response Processes

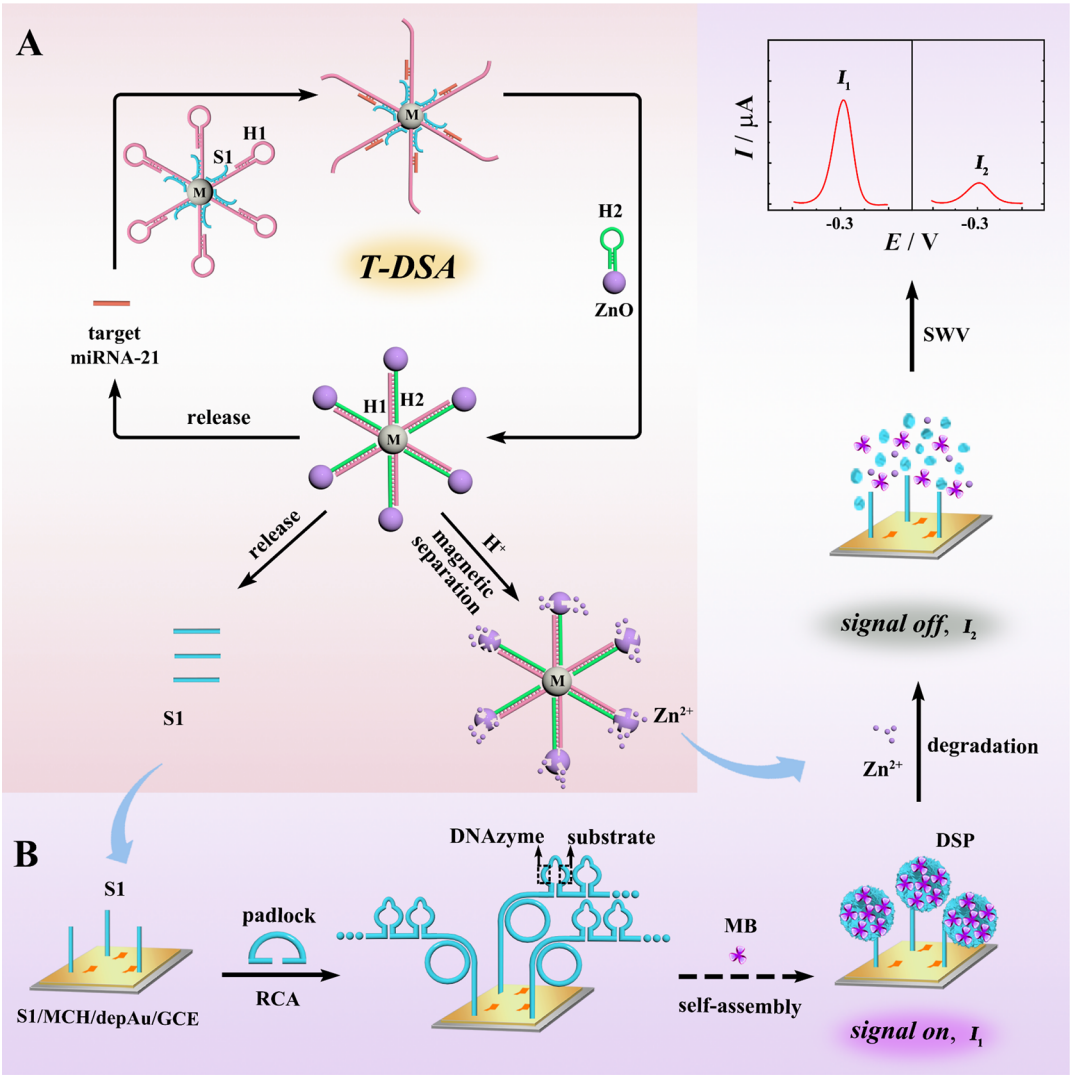

spheres (DSP). As depicted in Scheme 1A, the T-DSA was built by cleverly combining target-triggered recycle amplification and acid dissolution, in which the small target miRNA-21 could convert numerous mimic targets DNA S1 and excess Zn^{2+}, respectively. When S1 was modified onto the electrode through Au−S bonding, the functional DNA nanosphere (DSP) could be generated in situ by rolling circle amplification (RCA) to effectively capture abundant signal tag methylene blue (MB) with a significant electrochemical signal (signal on, I_1). Then, in the presence of the excess cofactor Zn^{2+}, the functional DSP assembled by DNAzyme and substrate sequence could be degraded programmatically to effectively release MB and obtain a nearly constant low electrochemical response (signal off, I_2). As a result, by measuring the ratiometric response of I_1/I_2, target miRNA-21 could be sensitively and accurately quantified with a detection limit as low as the attomole level. Above all, this novel strategy presented a novel electrochemical ratiometric assay, which could be extended to detect other biomarkers and pave the way for the application in bioanalysis and disease diagnosis.

EXPERIMENTAL SECTION

Synthesis of ZnO Particles. A two-stage reaction process was employed to synthesize ZnO particles according to previous research studies with a slight modification.[26,27] At first, zinc acetate dehydrate (0.005 mol) was dispersed into 50 mL of DEG (diethylene glycol) and the resultant mixture was reacted at 160 °C in an oil bath for 1 h to acquire a milk-like solution. This solution was then cooled down to room temperature and centrifuged to obtain a supernatant as a seeding solution for further reaction. In a classic synthesis process, another reaction solution of 50 mL of DEG and 0.005 mol of zinc acetate dehydrate was heated to 130 °C, and then the seeding solution obtained in the first step was added into this hot solution. Afterward, the temperature of the resulting solution was rapidly heated to 160 °C and further kept at this temperature for 1.5 h to generate ZnO particles. Then, the acquired ZnO particles were collected for later use after centrifugation and abstersion several times and finally dried in a vacuum at 60 °C for 12 h.

Preparation of H1/S1/MBs and H2/ZnO. In order to prepare H1/S1/MBs, H1 (2.5 μM, 125 μL) was first hybridized with S1 (2.5 μM, 125 μL) at 37 °C for 2 h to

https://doi.org/10.1021/acs.analchem.2c00190
Anal. Chem. 2022, 94, 5167−5172

generate the H1/S1 structure. Next, 40 mM EDC (*N*-(3-dimethylaminopropyl)-*N*′-ethylcarbodiimide hydrochloride) was injected into 250 μL of MBs (magnetic nanobeads) for 45 min to activate the carboxylic groups of MBs. Then, a mixture of 10 mM NHS (*N*-hydroxy succinimide) and the obtained H1/S1 was introduced to the aforesaid carboxylated MBs and stirred for 2 h. Sequentially, the prepared H1/S1/MBs was dispersed in 250 μL of Tris−HCl buffer after magnetic separation and abstersion.

Preparation of H2/ZnO was realized by conjugating the thiolated H2 onto amine-functionalized ZnO particles. First, the amino-functionalized ZnO particles were formed as follows: ZnO particles (0.05 g) was resuspended in 1 mL of amino reagent APTES under ultrasonication to get a homogeneous solution. Then, this mixture was vigorously stirred and heated to 100 °C for 5 h to introduce the amino group on the surface of ZnO particles. Afterward, 25 μL of 50 mM DTT (dithiothreitol) was introduced into 2.5 μM H2 (250 μL) at room temperature for 1 h to eliminate the S−S bond. Subsequently, amine-functionalized ZnO particles (250 μL) were activated by 15 μL of 20 mM SPDP (*N*-succinimidyl-3-(2-pyridyldithiol) propionate) for 1.5 h at 25 °C. Moreover, we used the centrifugal filter (Ultracel-30K membrane, Millipore) to remove superfluous SPDP and DTT. Finally, H2/ZnO was obtained after mixing the pretreated H2 and amine-functionalized ZnO particles at 25 °C for 2 h.

Target-Induced Dual Signal Amplification. The processes of target-induced dual signal amplification (T-DSA) were as follows. Primarily, the target miRNA-21 (50 μL) was mixed with 20 μL of H1/S1/MBs at 37 °C for 2 h, in which the DNA hairpin H1 was opened by target miRNA-21 to expose sticky ends for further hybridization. Then, 20 μL of H2/ZnO was introduced into the above mixture at 37 °C for 2 h. During the period, the hybridization of H1 and H2 by chain displacement reaction could release miRNA-21 for the next cycle. Afterward, the abundant mimic target DNA S1 and H1/MBs-H2/ZnO were obtained after multiple cycles. Finally, 40 μL of Tris−HCl including HCl (pH = 5) was injected into H1/MBs-H2/ZnO for dissolving ZnO particles into another mimic target Zn^{2+}, which was then collected after magnetic separation and stored at 4 °C for further use.

RESULTS AND DISCUSSION

Native Polyacrylamide Gel Electrophoresis (PAGE). PAGE was executed to demonstrate the feasibility of this proposed strategy. As shown in Figure 1A, miRNA-21, S1, H1, H2, and padlock all exhibited a distinct single band in lanes 1, 2, 3, 6, and 7, respectively. The band of the miRNA-21/H1/S1 hybrids was presented in lane 4, which was confirmed by its band running slower than those of miRNA-21 (lane 1), S1 (lane 2), and H1 (lane 3) separately. The table hybridization of H1 with H2 migrated slower in lane 5 with a long oligonucleotide sequence, which manifested that H2 could fully hybridize with H1. As expected, an apparent band appeared on the top of lane 8, indicating the successful formation of RCA-generated DNA nanospheres (DSP) in the presence of miRNA-21. When cofactor Zn^{2+} was added into the DSP, an obvious band with fast mobility was observed in lane 9, which demonstrated that Zn^{2+} successfully triggered the DNAzyme cleavage of DSP and further proved the feasibility of this strategy.

Characterization of the Prepared ZnO Particles and DNA Nanospheres. Scanning electron microscopy (SEM) and atomic force microscopy (AFM) were applied to characterize the prepared ZnO particles and the DNA nanospheres (DSP), respectively. The SEM images of the obtained ZnO are demonstrated in Figure 2A,B, which exhibited a uniform spherical morphology with an average size of ∼150 nm. To further verify the successful synthesis of ZnO, EDS mapping was utilized to investigate the distribution of various elements. As expected, the Zn and O elements exhibited dispersed spherical particles in Figure 2C,D,

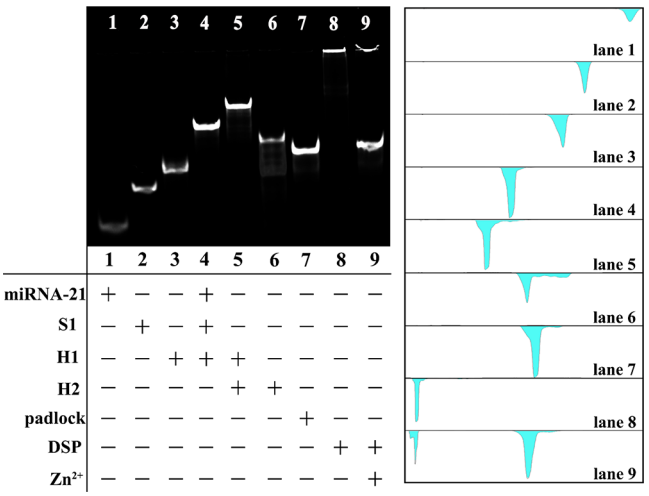

Figure 1. (A) PAGE analysis of the proposed strategy: lane 1: miRNA-21; lane 2: S1; lane 3: H1; lane 4: miRNA-21 + H1 + S1; lane 5: H1 + H2; lane 6: H2; lane 7: padlock; lane 8: DSP; lane 9: DSP + Zn^{2+}.

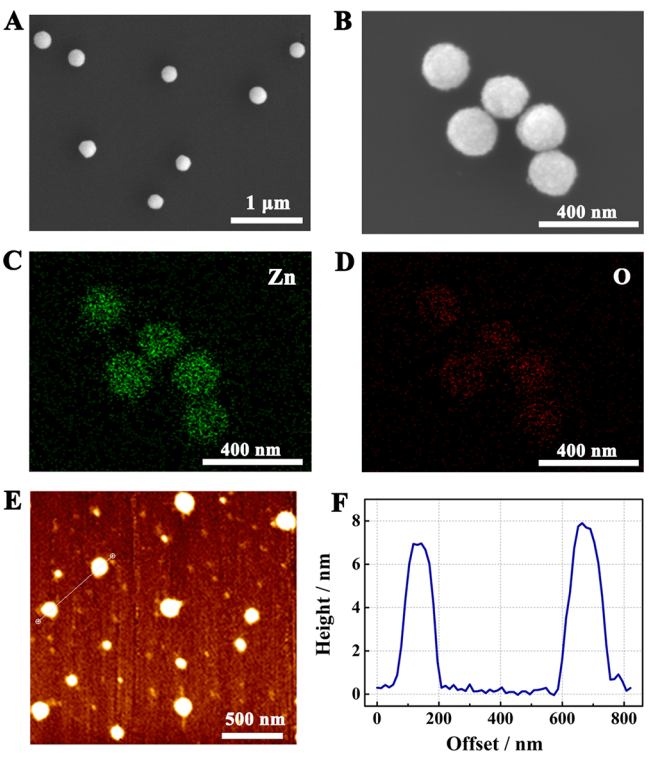

Figure 2. (A, B) SEM images of ZnO particles and the mapping images of ZnO particles showing the elemental distribution of (C) Zn and (D) O. (E) AFM image and (F) height analysis of the DSP (scale bars: 500 nm).

https://doi.org/10.1021/acs.analchem.2c00190
Anal. Chem. 2022, 94, 5167−5172

respectively. Moreover, the AFM image clearly exhibited the spherical configuration of the prepared DSP (Figure 2E) with ~7.5 nm height (Figure 2F). All these results indicated the production of the ZnO particles and DSP.

Feasibility of the Proposed Biosensor. In order to verify the feasibility of the proposed sensing strategy, the SWV responses were measured, as shown in Figure 3. As expected, in

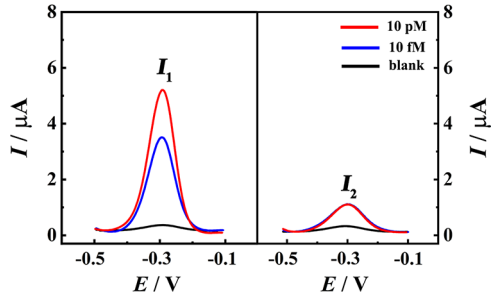

Figure 3. SWV measurements of MB for miRNA-21 detection with the proposed biosensor: in the presence of miRNA-21 (10 pM and 10 fM) and in the absence of miRNA-21 (blank).

the absence of a target, the oxidative peaks (I_1 and I_2) generated by the electrochemical signal tag MB (−0.3 V) were negligible (blank). Oppositely, the different concentrations of target miRNA-21 (10 pM and 10 fM) were introduced into the proposed sensing platform, resulting in the obvious peaks of I_1 (signal on) and the nearly constant peaks of I_2 (signal off). The above phenomena illustrated that S1 could induce the RCA reaction to generate negatively charged DSP to immobilize positively charged MB for a significant electrochemical signal and the excess Zn^{2+} could trigger the DNAzyme-catalyzed cleavage of DSP to release MB for an almost constant electrochemical signal. These results corroborate the feasibility of the novel ratiometric electrochemical strategy.

Optimization of the Detection Conditions. Some crucial experimental parameter conditions such as solution concentration and pH had been optimized to acquire the optimal detection conditions of the proposed biosensor. First, the concentration of MB was one of the most important factors affecting the sensitivity of the sensing platform. According to Figure 4A, as the concentration of MB changed from 10 to 60

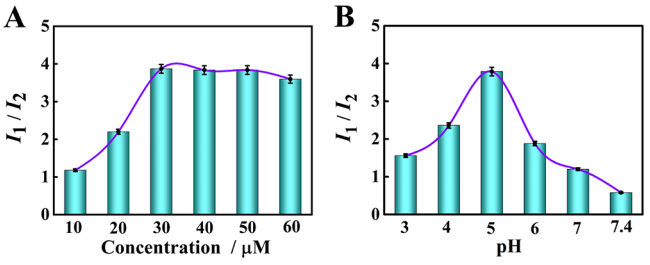

Figure 4. (A) Optimum concentration of MB and (B) pH of ZnO dissolution. The electrochemical signals were obtained with 100 fM miRNA-21. Error bars: SD, n = 3.

μM, the SWV response value of I_1/I_2 increased along with the increment of the MB concentration and stabilized after 30 μM. Thus, the optimal concentration of MB of 30 μM was chosen for further investigation.

Then, the pH of ZnO dissolution in this system affected the total amount of the dissolved Zn^{2+} ions, which further affected the DNAzyme-catalyzed cleavage of DSP for MB release. According to Figure 4B, the maximal electrochemical response was obtained at pH 5, which showed that pH 5 was used for ZnO dissolution in this system.

Analytical Performance. To assess the analytical performance of the ratiometric electrochemical biosensor, various concentrations of miRNA-21 were measured by SWV under the optimized conditions. According to Figure 5A, as the concentration of miRNA-21 increased, the SWV responses of I_1 increased significantly, while the peak current of I_2 did not change nearly. Therefore, the response value of I_1/I_2 gradually increased as the concentrations of miRNA-21 augmented. Furthermore, the ratio response of I_1/I_2 depended on the logarithm of miRNA-21 concentration over a range from 100 aM to 1 nM (Figure 5B). Also, the regression equation was $I_1/I_2 = 0.4988 \lg c_{\text{miRNA-21}} + 2.607$ with a correlation coefficient of 0.9986. Additionally, by comparison of the analytical performances for miRNA detection among different test platforms (Table 1), the proposed biosensor possessed an outstanding sensing performance with a detection limit down to 26.7 aM (S/N = 3), which illustrated that the proposed strategy had potential applications in sensitive biomedical detection.

Specificity and Stability of the Biosensor. Specificity is a pivotal criterion to assess biosensors and offers information about the anti-interference ability of the proposed sensing platform. For this purpose, some typical interferences involving miRNA-141, miRNA-203a, and miRNA-126 were used to evaluate the specificity of this system. The concentration of target miRNA-21 was 100-fold lower than the interference concentrations. As displayed in Figure 6A, only miRNA-21 and the mixture containing miRNA-21 could produce a significant I_1/I_2 response, while the current responses generated by other interferences were almost the same as that of the blank control. This result shows that the proposed system possessed an outstanding specificity for the monitoring of a specific biomarker. Additionally, the developed biosensors were also stored at 4 °C and assayed every 5 days to study the stability (Figure 6B). Significantly, the I_1/I_2 value of the biosensor still maintained 91.7% of its initial value after 20 days, illustrating an excellent stability of our ratiometric electrochemical sensing platform.

Reproducibility of the Biosensor. The ratiometric sensors are generally expected to possess a better reliability and reproducibility. Thus, the reproducibility of traditional non-ratiometric and our novel ratiometric electrochemical biosensors were compared under the same conditions. For the non-ratiometric biosensor, I_1 displayed a large fluctuation with an average of 4.683 μA and an RSD of 12.2% (Figure 7A). However, the fluctuations of I_1/I_2 values in the proposed sensing platform were notably decreased with an average of 3.521 μA and RSD of 3.1% (Figure 7B), indicating that this ratiometric strategy was more reproducible and robust than that of the classical non-ratiometric biosensors.

Application of the Proposed Biosensor in Cell Lysates. In order to validate the ability of the proposed biosensor for sensitive detection of miRNA-21 in practical samples, diverse cell lines including the MCF-7 cells with a highly overexpressed level of miRNA-21 and HeLa cells with low expression of miRNA-21 were employed for performance analysis. According to Figure 8, with the number of MCF-7 cells augmenting from 10^1 to 10^5, the I_1/I_2 value distinctly increased for the detection of miRNA-21. However, the low I_1/I_2 value and slow growth were observed with the intensive

https://doi.org/10.1021/acs.analchem.2c00190
Anal. Chem. 2022, 94, 5167−5172

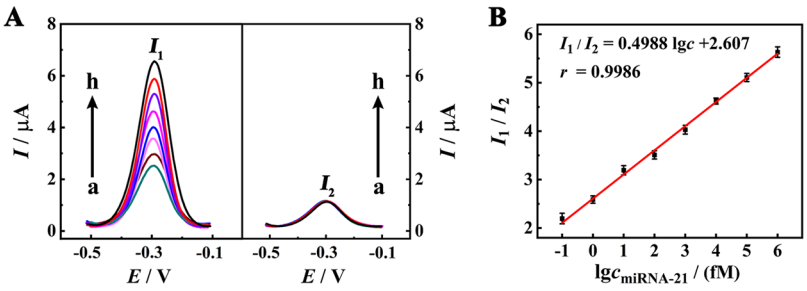

Figure 5. (A) SWV curves of the biosensor incubated with various concentrations of miRNA-21 (from curve a to curve h): 100 aM, 1 fM, 10 fM, 100 fM, 1 pM, 10 pM, 100 pM, and 1 nM. (B) Linear relationship between the ratio value of I_1/I_2 and logarithm of miRNA-21 concentrations.

Table 1. Comparison of the Proposed Biosensor with Other Reported Works for miRNA Detection

detection method	detection limit	linear range	ref
photoacoustic imaging	11.69 pM	10 pM to 100 nM	28
fluorescence	2.14 fM	2−40 pM	29
fluorescence	680 pM	1−100 nM	30
electrochemiluminescence	6.6 fM	10 fM to 0.1 nM	31
electrochemistry	2.2 fM	5 fm to 100 pM	32
electrochemistry	0.25 fM	0.5 fM to 100 nM	33
electrochemistry	26.7 aM	100 aM to 1 nM	this work

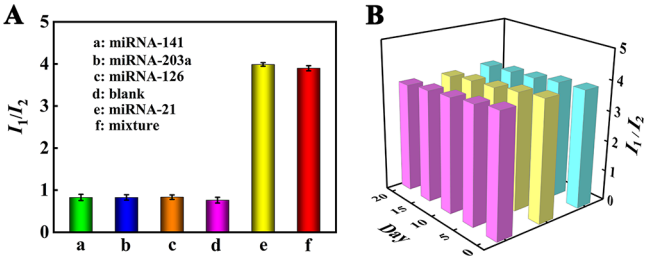

Figure 6. (A) Specificity of the strategy toward target miRNA-21 (100 fM) against other interfering miRNAs (each at 10 pM) and blank. (B) Stability of the sensing platform (100 fM miRNA-21) in the freezer.

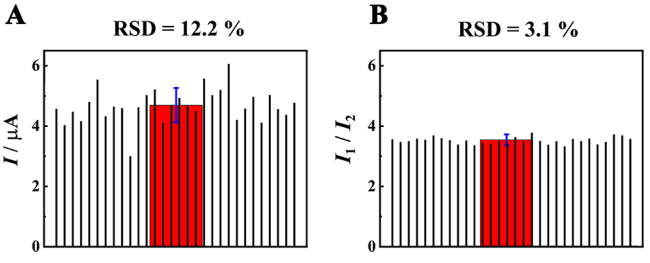

Figure 7. Reproducibility of (A) the non-ratiometric and (B) ratiometric biosensors toward target miRNA-21 (100 fM) separately. The black and red histograms displayed the electrochemical responses of 30 parallel measurements and the corresponding average responses, respectively.

numbers of Hela cells, indicating that the miRNA-21 level expressed in HeLa cells was low. These results are consistent with the previous research studies,[34,35] which illustrated that the proposed biosensor might have potential applications for biomolecule detection and cancers diagnosis.

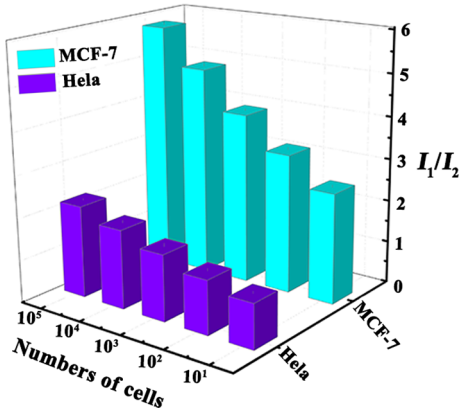

Figure 8. Practical analysis of miRNA-21 from diverse cell lysates.

CONCLUSIONS

In summary, under the help of an innovative target-induced dual signal amplification (T-DSA), a high-performance ratiometric electrochemical biosensor was proposed for ultrasensitive and accurate detection of miRNA-21 with methylene blue (MB) as the only one signal tag. First, our strategy could only use merely one electrochemical tag to effectively prevent the false positive responses from the non-ideal upright state of DNA probes connected to electrodes in the conventional distance-dependent signal adjustment ratiometric biosensors with two different signal tags. Second, the detection sensitivity of this biosensor was remarkably heightened with the assistance of the intelligent T-DSA recycle and RCA reaction. Additionally, this novel ratiometric strategy that we designed here might be considered as a widespread candidate for accurate and ultrasensitive detection of different biomarkers, which could provide some useful information for disease analysis and biological diagnosis.

ASSOCIATED CONTENT

Supporting Information

The Supporting Information is available free of charge at https://pubs.acs.org/doi/10.1021/acs.analchem.2c00190.

Materials and reagents; apparatus and measurements; fabrication of the modified electrodes; polyacrylamide gel electrophoresis; cell culture and total RNA extraction; and electrochemical characterization of the modified electrode (PDF)

https://doi.org/10.1021/acs.analchem.2c00190
Anal. Chem. 2022, 94, 5167−5172

AUTHOR INFORMATION

Corresponding Authors

Yaqin Chai − *Key Laboratory of Luminescence Analysis and Molecular Sensing (Southwest University), Ministry of Education, College of Chemistry and Chemical Engineering, Southwest University, Chongqing 400715, PR China;* orcid.org/0000-0003-4392-9592; Email: yqchai@swu.edu.cn

Ruo Yuan − *Key Laboratory of Luminescence Analysis and Molecular Sensing (Southwest University), Ministry of Education, College of Chemistry and Chemical Engineering, Southwest University, Chongqing 400715, PR China;* orcid.org/0000-0003-3664-6236; Phone: +86-23-68252277; Email: yuanruo@swu.edu.cn; Fax: +86-23-6825317

Authors

Lingqi Kong − *Key Laboratory of Luminescence Analysis and Molecular Sensing (Southwest University), Ministry of Education, College of Chemistry and Chemical Engineering, Southwest University, Chongqing 400715, PR China*

Hao Li − *Key Laboratory of Luminescence Analysis and Molecular Sensing (Southwest University), Ministry of Education, College of Chemistry and Chemical Engineering, Southwest University, Chongqing 400715, PR China*

Xiaolong Zhang − *Key Laboratory of Luminescence Analysis and Molecular Sensing (Southwest University), Ministry of Education, College of Chemistry and Chemical Engineering, Southwest University, Chongqing 400715, PR China*

Ying Zhuo − *Key Laboratory of Luminescence Analysis and Molecular Sensing (Southwest University), Ministry of Education, College of Chemistry and Chemical Engineering, Southwest University, Chongqing 400715, PR China;* orcid.org/0000-0002-4491-1186

Complete contact information is available at: https://pubs.acs.org/10.1021/acs.analchem.2c00190

Notes

The authors declare no competing financial interest.

ACKNOWLEDGMENTS

This work was financially supported by the NNSF of China (22174113, 22176153, and 21974108) and the Fundamental Research Funds for the Central Universities (XDJK2019B022), China.

REFERENCES

(1) Boon, R. A.; Iekushi, K.; Lechner, S.; Seeger, T.; Fischer, A.; Heydt, S.; Kaluza, D.; Tréguer, K.; Carmona, G.; Bonauer, A.; Horrevoets, A. J. G.; Didier, N.; Girmatsion, Z.; Biliczki, P.; Ehrlich, J. R.; Katus, H. A.; Müller, O. J.; Potente, M.; Zeiher, A. M.; Hermeking, H.; Dimmeler, S. *Nature* **2013**, *495*, 107−110.

(2) Brosnan, C. A.; Palmer, A. J.; Zuryn, S. *Nat. Commun.* **2021**, *12*, 2194.

(3) Zhao, J.; Li, Z.; Shao, Y.; Hu, W.; Li, L. *Angew. Chem., Int. Ed.* **2021**, *60*, 17937−17941.

(4) Zhou, W.-J.; Li, H.; Zhang, K.-K.; Wang, F.; Chu, X.; Jiang, J.-H. *J. Am. Chem. Soc.* **2021**, *143*, 14394−14401.

(5) Hao, M.; Miao, P.; Wang, Y.; Wang, W.; Ge, S.; Yu, X.; Hu, X.-X.; Ding, B.; Zhang, J.; Yan, M. *Anal. Chem.* **2021**, *93*, 11251−11258.

(6) He, P.; Han, W.; Bi, C.; Song, W.; Niu, S.; Zhou, H.; Zhang, X. *ACS Nano* **2021**, *15*, 6961−6976.

(7) Zhu, Y.-L.; Lian, Y.-M.; Wang, J.-K.; Chen, Z.-P.; Yu, R.-Q. *Anal. Chem.* **2021**, *93*, 5839−5848.

(8) Zhang, Y.; Chen, W.; Fang, Y.; Zhang, X.; Liu, Y.; Ju, H. *J. Am. Chem. Soc.* **2021**, *143*, 15233−15242.

(9) Ning, Z.; Yang, E.; Zheng, Y.; Chen, M.; Wu, G.; Zhang, Y.; Shen, Y. *Anal. Chem.* **2021**, *93*, 8971−8977.

(10) Peng, H.; Newbigging, A. M.; Reid, M. S.; Uppal, J. S.; Xu, J.; Zhang, H.; Le, X. C. *Anal. Chem.* **2021**, *93*, 292−308.

(11) Lu, X.; Hu, C.; Jia, D.; Fan, W.; Ren, W.; Liu, C. *Nano Lett.* **2021**, *21*, 6718−6724.

(12) Liu, S.; Wang, X.; Yu, X.; Cheng, Q.; Johnson, L. T.; Chatterjee, S.; Zhang, D.; Lee, S. M.; Sun, Y.; Lin, T.-C.; Liu, J. L.; Siegwart, D. J. *J. Am. Chem. Soc.* **2021**, *143*, 21321−21330.

(13) Zhang, P.; Ouyang, Y.; Sohn, Y. S.; Nechushtai, R.; Pikarsky, E.; Fan, C.; Willner, I. *ACS Nano* **2021**, *15*, 6645−6657.

(14) Jiao, K.; Yan, Q.; Guo, L.; Qu, Z.; Cao, S.; Chen, X.; Li, Q.; Zhu, Y.; Li, J.; Wang, L.; Fan, C.; Wang, F. *Angew. Chem., Int. Ed.* **2021**, *60*, 14438−14445.

(15) Zhang, D.; Wang, K.; Wei, W.; Liu, Y.; Liu, S. *Anal. Chem.* **2021**, *93*, 9521−9530.

(16) Su, J.; Wu, F.; Xia, H.; Wu, Y.; Liu, S. *Chem. Sci.* **2020**, *11*, 80−86.

(17) Wu, J.; Zhou, X.; Li, P.; Lin, X.; Wang, J.; Hu, Z.; Zhang, P.; Chen, D.; Cai, H.; Niessner, R.; Haisch, C.; Sun, P.; Zheng, Y.; Jiang, Z.; Zhou, H. *Anal. Chem.* **2021**, *93*, 8799−8809.

(18) Li, Y.; Chang, Y.; Ma, J.; Wu, Z.; Yuan, R.; Chai, Y. *Anal. Chem.* **2019**, *91*, 6127−6133.

(19) Zhu, L.; Zhang, M.; Ye, J.; Yan, M.; Zhu, Q.; Huang, J.; Yang, X. *Anal. Chem.* **2020**, *92*, 8614−8622.

(20) Yang, L.; Yin, X.; An, B.; Li, F. *Anal. Chem.* **2021**, *93*, 1709−1716.

(21) Zhang, Q.; Fu, Y.; Xiao, K.; Du, C.; Zhang, X.; Chen, J. *Anal. Chem.* **2021**, *93*, 6801−6807.

(22) Xiong, E.; Li, Z.; Zhang, X.; Zhou, J.; Yan, X.; Liu, Y.; Chen, J. *Anal. Chem.* **2017**, *89*, 8830−8835.

(23) Monserud, J. H.; Schwartz, D. K. *ACS Nano* **2014**, *8*, 4488−4499.

(24) Gu, Q.; Nanney, W.; Cao, H. H.; Wang, H.; Ye, T. Single Molecule Profiling of Molecular Recognition at a Model Electrochemical Biosensor. 2018, *140*, 14134−14143, DOI: 10.1021/jacs.8b07325.

(25) Kékedy-Nagy; Ferapontova, E. E. *Angew. Chem., Int. Ed.* **2019**, *58*, 3048−3052.

(26) Ji, W.; Li, L.; Song, W.; Wang, X.; Zhao, B.; Ozaki, Y. *Angew. Chem., Int. Ed.* **2019**, *58*, 14452−14456.

(27) Seelig, E. W.; Tang, B.; Yamilov, A.; Cao, H.; Chang, R. P. H. *Mater. Chem. Phys.* **2003**, *80*, 257−263.

(28) Zhang, K.; Meng, X.; Yang, Z.; Cao, Y.; Cheng, Y.; Wang, D.; Lu, H.; Shi, Z.; Dong, H.; Zhang, X. *Adv. Mater.* **2019**, *31*, 1807888.

(29) Wang, J.; Wang, D.-X.; Ma, J.-Y.; Wang, Y.-X.; Kong, D.-M. *Chem. Sci.* **2019**, *10*, 9758−9767.

(30) Yang, F.; Cheng, Y.; Cao, Y.; Dong, H.; Lu, H.; Zhang, K.; Meng, X.; Liu, C.; Zhang, X. *Chem. Sci.* **2019**, *10*, 1709−1715.

(31) Zhang, P.; Jiang, J.; Yuan, R.; Zhuo, Y.; Chai, Y. *J. Am. Chem. Soc.* **2018**, *140*, 9361−9364.

(32) Zhou, H.; Zhang, J.; Li, B.; Liu, J.; Xu, J.-J.; Chen, H.-Y. *Anal. Chem.* **2021**, *93*, 6120−6127.

(33) Zhang, X.; Yang, Z.; Chang, Y.; Liu, D.; Li, Y.; Chai, Y.; Zhuo, Y.; Yuan, R. *Chem. Sci.* **2020**, *11*, 148−153.

(34) Gong, X.; Li, R.; Wang, J.; Wei, J.; Ma, K.; Liu, X.; Wang, F. *Angew. Chem., Int. Ed.* **2020**, *59*, 21648−21655.

(35) Li, S.; Xu, L.; Ma, W.; Wu, X.; Sun, M.; Kuang, H.; Wang, L.; Kotov, N. A.; Xu, C. *J. Am. Chem. Soc.* **2016**, *138*, 306−312.